ACS NANO

www.acsnano.org

ARTICLE

μeV-Deep Neutron Bound States in Nanocrystals

Hao Tang, Guoqing Wang, Paola Cappellaro, and Ju Li*

Cite This: *ACS Nano* 2024, 18, 9063−9070

Read Online

ACCESS | Metrics & More | Article Recommendations | Supporting Information

ABSTRACT: **The strong nuclear force gives rise to the widely studied neutron scattering states and MeV-energy nuclear bound states. Whether this same interaction could lead to low-energy bound states for a neutron in the nuclear force field of a cluster of nuclei is an open question. Here, we computationally demonstrate the existence of μeV-level neutronic bound states originating from the strong interactions in nanocrystals with a spatial extent of tens of nanometers. These negative-energy neutron wave functions depend on the size, dimension, and nuclear spin polarization of the nanoparticles, providing engineering degrees of freedom for the artificial neutronic "molecule".**

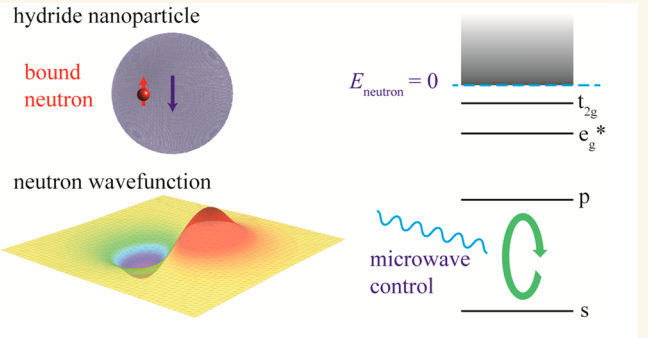

KEYWORDS: *ultracold neutron, nanoparticle, bound states, strong interaction, quantum control*

INTRODUCTION

Neutron scattering is a widely used technique to characterize materials' structure and dynamics.[1] In neutron scattering, the interference of neutron's positive-energy scattering states in a cluster of nuclei is utilized to probe the atomic configuration,[2] magnetic structures,[3] and ionic motion.[4] Besides scattering states, the strong nuclear interaction between neutron and nuclei can also trap a neutron in femtometer-scale bound states, known as the radiative neutron capture.[5] Such bound states have MeV-scale binding energy, where the neutron and nucleus combine into another isotope and emit γ-photon.[6] The energy spectra of the neutron, therefore, include the continuum spectra from scattering states covering the positive energy range and the discrete lines from bound states with ∼MeV deep negative energy. The energy gap between the deeply negative and positive energy spectra contains no bound states[7] if the neutron just interacts with a single nucleus due to the short-range nature of the strong nuclear interaction.[8,9] However, it is unknown to us whether a neutron interacting with a cluster of nuclei can have low-energy bound states. Intuitively, the neutron eigenstates of different nuclei interact with each other and form delocalized eigenstates, in analogy to how the linear combination of atomic orbitals (LCAO) forms molecular orbitals lower in energy than the isolated atomic orbitals.[10] It is, therefore, intriguing to probe whether there are long-lived discrete weakly bound states of neutrons, localized around a collection of nuclei, e.g., nanoparticles and nanowires. We define the negative-energy neutronic states with a 10 nm-scale broadening of the "molecular neutronic" states. Such weakly bound neutron states, if they exist, would provide a platform for designing neutron eigenfunction by controlling the material configuration and for probing the strong nuclear force by low-energy neutrons. For example, the molecular neutronic states can be used in probing the nuclei's neutron scattering and absorption cross sections,[11] neutron electric dipole moment,[12,13] as well as neutron bound-state β^--decay[14] under the low-energy limit, which contains critical information about the strong force, one of the four fundamental forces of nature.

In this work, we demonstrate the existence of the molecular neutronic state in hydrogen-containing nanocrystals by analytical derivation and computational simulations. Essentially, the multicenter superposition of positive-energy scattering states can form a negative-energy weakly bound state. Different from the MeV neutron bound states whose properties are set by the fixed isotope properties,[6] the energy levels and wave functions of molecular neutronic states can be engineered by the host nanocrystal's size and shape. As the molecular neutronic state is similar to the electronic state in quantum dots,[15] we call the system hosting such states "neutronic quantum dot" (NQD).

Received: December 21, 2023
Revised: February 13, 2024
Accepted: February 27, 2024
Published: March 15, 2024

RESULTS AND DISCUSSION

Theory. We use Green's function formalism and direct numerical calculations to demonstrate the existence of low-energy bound neutron states. The neutron moves in a nuclear force potential $V(\vec{r}) = \sum_i v_i(\vec{r})$, where $v_i(\vec{r})$ is the potential of the ith nucleus located at $\vec{R}_i$ (i = 1, 2, ..., N, with N being the nuclei in the system). Solving for neutron states in the NQD encounters a multiscale challenge:[16] the strong interaction v_i is localized to the femtometer length scale, while the interatomic distance $\vec{R}_i - \vec{R}_j$ is of the length scale of Å, exhibiting a separation of 5 orders of magnitude. That makes it prohibitively expensive to directly discretize the Schrödinger equation on a uniform spatial grid. In order to bypass this problem, we use the Green function formalism to show that the concept of Fermi pseudo potential[17] used in neutron scattering can also be applied to the molecular neutronic states, which coarse-grains the detailed fm-scale features into the scattering length.[11]

The bound-state wave function $\psi(\vec{r})$ with an eigenenergy $E < 0$ can be obtained from an integral equation[18]

$$\psi(\vec{r}) = -\int \frac{2m_n}{\hbar^2} V(\vec{r}\,')G(\vec{r}, \vec{r}\,'; E)\psi(\vec{r}\,')\mathrm{d}r'^3 \tag{1}$$

over the single neutron Green function $G(\vec{r}, \vec{r}\,'; E) = \frac{e^{-\kappa|\vec{r}-\vec{r}\,'|}}{4\pi|\vec{r}-\vec{r}\,'|}$ satisfying $[\kappa^2 - \nabla^2]G(\vec{r},\vec{r}\,';E) = \delta(\vec{r} - \vec{r}\,')$, with $\kappa = \sqrt{-2m_nE/\hbar^2}$, m_n is the neutron mass and $\hbar$ is the reduced Planck constant. As the support of $V(\vec{r})$ is localized to the femtometer-neighborhoods around the nuclei positions, the integral can be rewritten as a sum of local integrals around each nucleus. Depending on whether $\vec{r}$ is close to a nucleus, the integral eq 1 can be rewritten as

$$\psi(\vec{r}) \simeq \begin{cases} -\sum_i G(\vec{r}, \vec{R}_i; E)\int_{\Omega_i} \frac{2m_n v_i(\vec{r}\,')}{\hbar^2}\psi(\vec{r}\,')\mathrm{d}r'^3, \ (\forall\, i|\vec{r} - \vec{R}_i| \gg fm) \\ -\sum_{i\neq j} G(\vec{r}, \vec{R}_i; E)\int_{\Omega_i} \frac{2m_n v_i(\vec{r}\,')}{\hbar^2}\psi(\vec{r}\,')\mathrm{d}r'^3 \\ \quad - \int_{\Omega_j} G(\vec{r}, \vec{r}\,'; E)\frac{2m_n v_j(\vec{r}\,')}{\hbar^2}\psi(\vec{r}\,')\mathrm{d}r'^3, \ (|\vec{r} - \vec{R}_j| \sim fm) \end{cases} \tag{2}$$

Here Ω_i is a spherical volume around the ith nucleus with a radius of the nuclear force range. In the first case, the position $\vec{r}$ is far from all nuclei; in the second case, the position $\vec{r}$ is ∼ fm close to that of $\vec{R}_j$. For all nuclei i subject to $|\vec{r} - \vec{R}_i| \gg$ fm, we applied the Green function approximation $G(\vec{r},\vec{r}\,';E)\,|_{\vec{r}\,'\in\Omega_i} \simeq G(\vec{r},\vec{R}_i;E)$. The detailed behavior of the wave function around the nuclei (including fm-scale oscillations) is uninfluential to the Å-scale spatial distribution of low-energy neutron states.[17] Therefore, we coarse-grain the wave function over an intermediate length scale fm $\ll D \ll$ Å and introduce the average wave function, $\overline{\psi}(\vec{r}) \equiv \frac{3}{4\pi D^3}\int_{|\vec{r}-\vec{r}\,'|<D}\psi(\vec{r}\,')\mathrm{d}r'^3$. The nuclei's influence on the average wave function can be described by the Fermi pseudo potential, $v_i^{PP}(\vec{r}) = \frac{2\pi\hbar^2}{m_n}\mathrm{Re}[b_i]\delta^D(\vec{r} - \vec{R}_i)$ $\left(\text{with } \delta^D(\vec{r}) = \frac{3}{4\pi D^3} \text{ if } |\vec{r}| < D \text{ and 0 elsewhere}\right)$,[17] whose strength is characterized by the real part of the scattering length b_i.[11] We prove (see Supporting Information (SI)[19−23] section I for details) that the following equation of the average wave function can be derived by integrating eq 2:

$$\overline{\psi}(\vec{r}) \simeq -\sum_{i,|\vec{r}-\vec{R}_i|\gg fm} \frac{e^{-\kappa|\vec{r}-\vec{R}_i|}}{|\vec{r} - \vec{R}_i|}\mathrm{Re}[b_i]\overline{\psi}(\vec{R}_i) \tag{3}$$

where the second term in the second case of eq 2 is proved to be negligible after integration. The scattering length is more frequently used to describe low-energy (compared to MeV) neutron scattering, where the neutron state has a near-zero positive energy. In our neutron bound state case, the neutron has a near-zero negative energy. The two situations share the same scattering length (see SI section S1 for details). The average wave function at nucleus positions $\vec{R}_i$, $\overline{\psi}_i \equiv \overline{\psi}(\vec{R}_i)$ can then be obtained by solving an eigenvalue problem

$$\overline{\psi}_i + \sum_{j\neq i} \frac{e^{-\kappa|\vec{R}_i-\vec{R}_j|}}{|\vec{R}_i - \vec{R}_j|}\mathrm{Re}[b_j]\overline{\psi}_j = 0 \tag{4}$$

simultaneously determining the wavevector κ and the binding energy $E_b \equiv \frac{\hbar^2\kappa^2}{2m_n}$. The molecular neutronic state exists if and only if eq 4 has a nonzero solution with $\kappa > 0$. Provided that a nucleus has a negative scattering length,[11] the condition can be satisfied when the size and density of the nuclear cluster exceed a threshold, thus, indicating the existence of a bound state. Because $\left|\frac{e^{-\kappa R_{ij}}}{R_{ij}}\mathrm{Re}[b_j]\right|$ is far smaller than 1 (where we define $R_{ij}\equiv|\vec{R}_i-\vec{R}_j|$), the equation can be satisfied only when the summation is over a large number of nuclei, so that the second term can cancel the first term. Details on the solutions of eq 4 are elaborated in Methods.

Energy Level and Eigenfunction. The existence of neutronic bound states thus requires negative scattering lengths, representing attractive forces to neutrons. Protons have a negative neutron scattering length with the largest magnitude among all isotopes when their nuclear spin is polarized opposite to that of the neutron.[11] Polarization of the nuclear spin of hydrogen nuclei can be achieved by various experimental techniques, including dynamic nuclear polarization (DNP)[24,25] and optical pumping.[26] In the following simulation, we assume that all hydrogen nuclear spins in the nuclear cluster are polarized in the same direction. We use LiH nanocrystal (Figure 1a), a widely studied hydrogen storage material,[27−29] as an exemplary system to demonstrate the existence of weakly bound neutronic states by solving eq 4 numerically. The nanocrystalline quantum dot (nanocrystal) is assumed to have a spherical shape with a radius R of tens of nanometers.[30,31] Both Li and H have an attractive nuclear force with neutrons,[11] creating the negative nuclear strong-force potential shown in Figure 1b. The binding energy levels of the bound states are then calculated as a function of the nanocrystal radius, as shown in Figure 1c. The existence of bound states requires the nanocrystal radius R to be larger than a critical value, R_c = 13 nm in the LiH case. Intuitively, that is because confining neutrons in a smaller-R NQD requires higher wavenumbers and thus kinetic energy, which makes the overall energy positive, so that the bound states can no longer exist. Larger R gives rise to multiple bound states with different symmetries (see Figure 1d), whose binding energies all increase monotonically with R. The neutronic d orbitals of LiH NQD split into t_{2g} (the 1d (*3, meaning 3-fold degeneracy) curve) and e_g^* orbitals (the 1d (*2) curve)

https://doi.org/10.1021/acsnano.3c12929
ACS Nano 2024, 18, 9063−9070

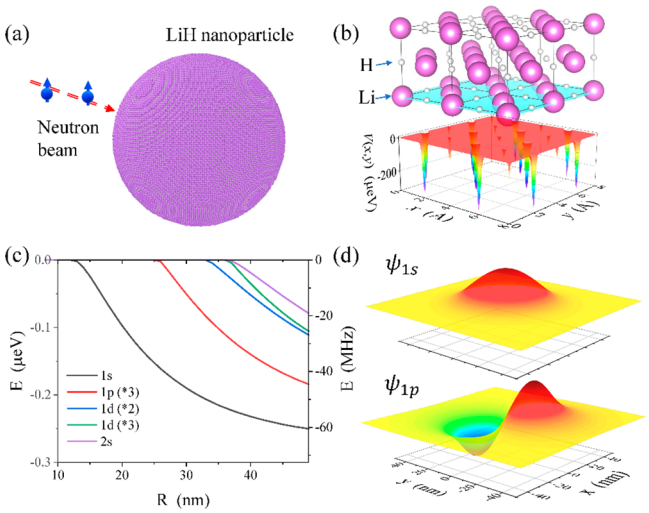

Figure 1. (a) Illustration of cold neutron bound states in a 30 nm radius LiH spherical nanocrystal. (b) Atomic structure (top) and nuclear force potential (bottom) of neutrons in LiH at zero temperature, where the hydrogen nuclear spins are fully polarized in the opposite direction with the neutrons. The nuclear force potential is smeared by the zero-point vibrations of nuclides to become a sum of picometer length scale Gaussians and visualized on the (100) canyon plane. (c) Binding energies of molecular neutronic states as a function of nanocrystal radius. The energy levels are denoted as 1s, 1p (3-fold degeneracy), 1d (*2, 2-fold degeneracy), 1d (*3, 3-fold degeneracy), and 2s from low to high. (d) Real part of the average eigenfunction $\bar{\psi}(\vec{r})$ of 1s and 1p states when R = 30 nm, plotted on a plane across the center of the sphere.

because the cubic lattice breaks the SO(3) symmetry of the spherically shaped nanocrystal.[32] The eigenfunctions corresponding to the first two energy levels, 1s and 1p, are plotted in Figure 1d. These neutronic eigenfunctions cover the whole nanocrystal and extend tens of nanometers into the vacuum. Moreover, the bound states and their transition frequencies can be engineered by the size and shape of the nanocrystal, providing additional tunability for quantum applications.

The binding energies of the molecular neutronic states depend on the size and dimensionality of the nanocrystal. The Γ-point neutron bound-state energy levels in the zero-dimensional LiH nanoparticle, one-dimensional LiH nanowire, and two-dimensional LiH thin film are shown in Figure 2a, b, and c, respectively. Multiple μeV-level bound states exist and exhibit stronger binding for larger system sizes (diameter for nanoparticle and nanowire, thickness for thin film) in all three systems. Systems with higher dimensions have a smaller minimal size to host a bound state and approach stronger binding at the same system size. Different from the nanoparticle case, a thin film with arbitrarily small thickness hosts bound states. That means the neutronic bound state can exist in 2D systems with atomic-scale thickness. The neutron bound states around the Γ point in three-dimensional LiH perfect crystal have a parabolic band dispersion, as shown in Figure 2d. The band structure is calculated by both eq 4 and a planewave basis expansion method, showing consistent results. The Γ-point energy in infinite LiH crystal is −0.33 μeV, which is the lower bound of the neutron energy levels in LiH. In the nanowire and thin film (Figure 2e,f), the bound state energy band splits into a series of sub-bands due to the quantum

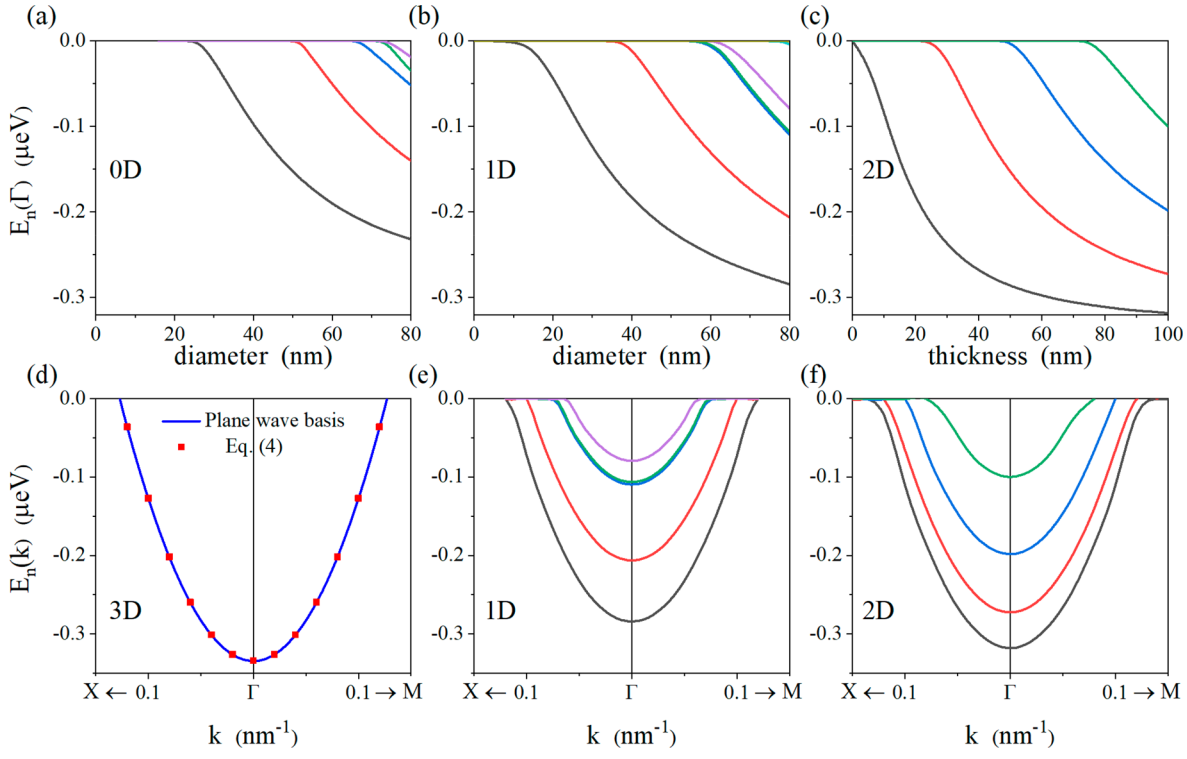

Figure 2. Bound neutron states in nanostructures with different dimensionality. Bound energy levels in LiH (a) zero-dimensional spherical nanoparticles, (b) one-dimensional cylindrical nanowire, and (c) two-dimensional thin film at T point as a function of the diameter of the nanoparticle, nanowire, and thickness of the thin film. (d) Neutron bound states band structure in perfect LiH crystal using eq 4 and a plane wave basis expansion method. (e) Neutron band structure in the 80 nm diameter spherical nanowire and (f) 100 nm thickness thin film. Throughout this figure, we assume hydrogen nuclear spins are fully polarized.

https://doi.org/10.1021/acsnano.3c12929
ACS Nano 2024, 18, 9063−9070

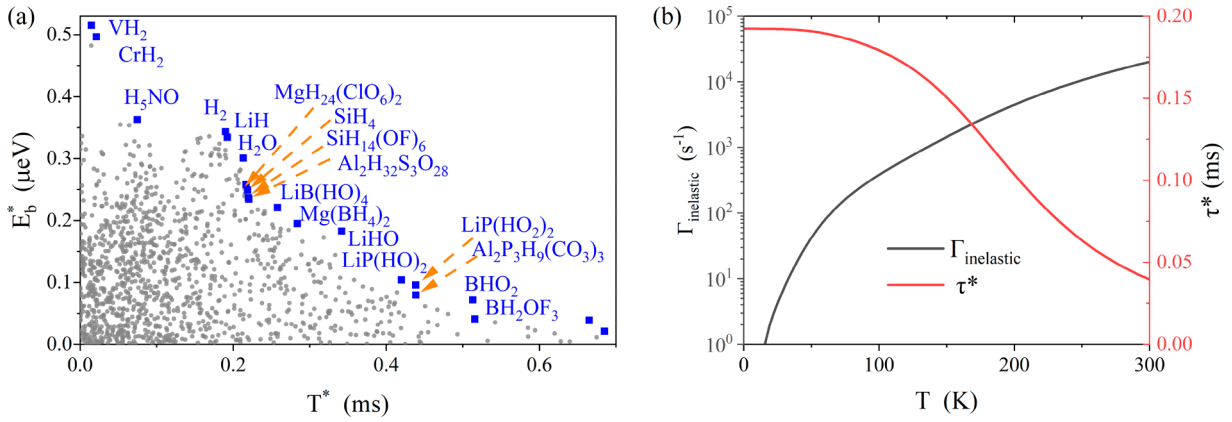

Figure 3. (a) Binding energy E_b^* and lifetime T^* of molecular neutronic states in different perfect hydride crystals at zero temperature. The crystals are selected from 10,409 hydride systems from the materials project database, and crystals satisfying Pareto optimality with respect to exhibiting large binding energy and lifetime are denoted as blue squares. (b) Inelastic neutron−phonon up-scattering rate and lifetime of neutron bound state as a function of temperature.

confinement, showing the same behavior as electron band structures in low-dimensional structures.

Under realistic conditions, the hydrogen nuclear spins in the host materials may not be completely polarized.[24,25] We verify that neutronic bound states can still exist under an incomplete but finite nuclear-spin polarization, as shown in Figure S2 in SI, section S4. If the polarization is incomplete but not far from fully polarized, then the bound state will have a slightly smaller binding energy than the complete polarization case. Therefore, the neutronic bound states are robust to a constant incomplete nuclear spin polarization. The nuclear spin polarization can also have temporal fluctuation, which adds random perturbation to the bounded neutron.[33] However, as the bound-state neutron wave function extends among millions of nuclei, it effectively only interacts with the average nuclear spin polarization. Although a single nuclear spin polarization can have evident fluctuation, the fluctuation of the average polarization of a large number of nuclear spins is likely small. Despite this, the temporal fluctuation of the average nuclear spin polarization depends on specific experimental conditions, which need to be evaluated case by case.

Being spin-1/2 Fermions like electrons, the many-neutron wave function $\Psi(\mathbf{x}_n^1,\mathbf{x}_n^2, ..., \mathbf{x}_n^N)$ of N identical neutrons, with $\mathbf{x}_n^i$ labeling both the position and spin of a neutron, must satisfy $\Psi(..,\mathbf{x}_n^i, ..., \mathbf{x}_n^j, ...) = -\Psi(..., \mathbf{x}_n^j, ..., \mathbf{x}_n^i, ...)$. The independent particle picture, an approximation of $\Psi(\mathbf{x}_n^1,\mathbf{x}_n^2, ..., \mathbf{x}_n^N)$, suggests that neutrons can fill up the NQD states in a "neutronic shell model" akin to the electronic shell filling in molecules, with the single-particle energy and degeneracy illustrated in Figures 1c and 2. The ground-state wave function is thus approximated by a Slater determinant of the N lowest-energy NQD spin−orbital states. With the QD size increasing to infinity, turning the nanostructure into a bulk material, we have computed that if all the bound states are occupied by neutrons all the way to $E = 0^-$, there will be a maximal mass gain of the LiH crystal by 6.8×10^{-6} % (68 ppb), which could be measurable experimentally. Also, unlike electrons, the neutron−neutron interaction between these delocalized NQD spin-orbitals is rather weak; thus, the many-neutron quantum state may be a good approximation of the noninteracting limit of a many-Fermion system and have some unique characteristics as a quantum information platform.

Lifetime of Neutron Bound States. A neutron trapped in a negative-energy state in materials can still undergo radioactive decay and turn into a proton, electron, and antineutrino,[34] or get upscattered in energy by lattice vibrations.[35] Besides the binding energy, the lifetime is also an important feature in characterizing the neutron bound state. Although neutrons interact weakly with the environment, their lifetimes are limited by the nuclear reaction probabilities that the weakly bound neutron is finally absorbed by H or Li to form D or ^{7}Li. The absorption of bound-state neutrons exists even when the nanoparticle is at zero temperature, so it gives an upper bound of a neutronic bound state's lifetime. In comparison, neutron upscattering by lattice vibrations does not happen at zero temperature but becomes dominant when the nanoparticle is at room temperature. In the following, we first show results on neutron capture and then phonon upscattering.

Neutron Absorption Lifetime. For a given infinite crystal, we define the ground-state binding energy as E_b^* and the ground-state neutron absorption lifetime (inverse of the neutron absorption rate) as T^*, which is the neutron bound state's lifetime at zero temperature (upper bound). They can be calculated as materials properties:

$$E_b^* = -\frac{2\pi\hbar^2}{m_n\Omega}\sum_i n_i \mathrm{Re}[b_i]$$

$$\frac{1}{T^*} = \lim_{E_k\to 0}\frac{1}{\Omega}\sum_i n_i\sigma_a^i(E_k)\sqrt{\frac{2E_k}{m_n}} \quad (5)$$

where Ω is the unit cell volume, n_i, b_i, and σ_a^i (E_k) are the number of i-type atoms in a unit cell, their scattering length, and neutron absorption cross section for neutron with a kinetic energy of E_k. Finite-size nanocrystal gives smaller binding energy E_b and longer neutron absorption lifetime T_{life}, but their product is bounded by an inequality (see SI, section S2 for derivations):

$$E_b T_{life} \le E_b^* T^* = -\frac{\hbar}{2}\frac{\mathrm{Im}[\sum_i n_i b_i]}{\mathrm{Re}[\sum_i n_i b_i]} \quad (6)$$

showing that increasing the neutron absorption lifetime may lead to a decrease in binding energy with the same combination of isotopes.

https://doi.org/10.1021/acsnano.3c12929
ACS Nano 2024, 18, 9063−9070

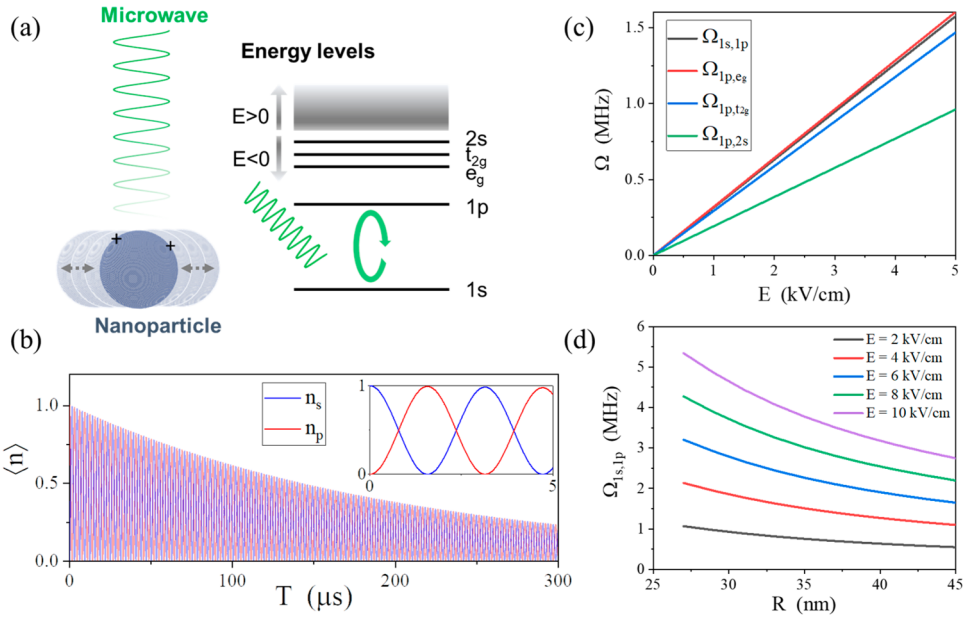

Figure 4. (a) Microwave control of neutron bound states in nanocrystals. The electric field of the microwave in resonance with 1s to 1p transition drives oscillations of charged nanocrystals and neutron states. (b) Rabi oscillation of neutronic 1s and 1p states (R = 40 nm, E = 1 kV/cm, V_{LiH} = 1 V). The average population of neutrons in the 1s state (n_s) and 1p state (n_p) is plotted as a function of time. (c) Rabi frequency of different transitions as a function of microwave electric field (R = 40 nm, V_{LiH} = 1 V). (d) Rabi frequency of 1s to 1p transition as a function of nanocrystal radius and electric field (V_{LiH} = 1 V).

The E_b^* and T^* of different crystals are shown in Figure 3, where the gray dots list all nonradioactive stable crystal structures from the Materials Project database that contain hydrogen and can host bound states.[36] The binding energies are at the level of μeV, corresponding to a required milli-Kelvin-level temperature, that is already realizable with the present ultracold neutron (UCN) technology.[37] The lifetime is at the level of 0.1−1 ms. In general, there is a trade-off between binding energy and lifetime. Materials satisfying Pareto optimality[38] (that means no material simultaneously has larger binding energy and longer lifetime than each selected material) are labeled by the blue points in Figure 3, forming a frontier curve of possible (E_b^*,T^*) combinations. A series of common hydrogen storage nanomaterials,[28] including MgH_2 (0.27 μeV, 0.19 ms) and $LiBH_4$ (0.27 μeV, 0.19 ms) also exhibit reasonably high E_b^* and T^*.

Neutron−Phonon Upscattering. Under experimental conditions, the nanoparticle can have a nonzero lattice temperature T, and lattice vibrations in the nanoparticle give rise to inelastic phonon scattering of the bound neutron, where it can absorb a phonon and gain energy.[35] As phonons typically have meV energy scale, it will eject the neutron out of the bound states, reducing the bound states' lifetime at increasing temperatures. The total upscattering rate from the neutron ground state in bulk crystal is derived using Fermi's golden rule:

$$\Gamma_{\text{upscattering}}(T) = \frac{\hbar^4}{2m_n^2}\frac{1}{\Omega_{u.c.}}\sum_{m,n}\int_{BZ} d^3k f_{B.E.}(\omega_{nk}, T)\frac{1}{M_{nk}^{u.c.}\omega_{nk}} \times \left|(\vec{k}+\vec{G}_m)\cdot\sum_{i\in u.c.}\vec{e}_{ij}^{\,0}b_i\right|^2 \delta\left(\frac{\hbar^2(\vec{k}+\vec{G}_m)^2}{2m_n} - E_0 - \hbar\omega_{nk}\right) \quad (7)$$

The meanings of symbols and detailed derivations are provided in SI, section S3. We numerically evaluate eq 7 for the neutronic bound states in the LiH crystal and obtain the temperature-dependent neutron upscattering rate, as shown in Figure 3b. The neutron upscattering rate is positively related to temperature and approaches 2.01×10^4 s^{-1} at 300 K, which is larger than the neutron nuclear absorption rate of 0.52×10^4 s^{-1} in the same setting. That means if the nanoparticle is not cooled below room temperature, the neutron upscattering will be the main limitation of the bound state's lifetime. The bound state's lifetime is evaluated as $\tau^* = \left(\frac{1}{T^*} + \Gamma_{\text{upscattering}}\right)^{-1}$ considering both neutron reaction and upscattering (Figure 3b). We notice that cooling the host material to liquid nitrogen temperature increases the bound state's lifetime τ^* to 0.186 ms, close to the zero-temperature limit of 0.192 ms. The phonon upscattering process also influences the lifetime of neutron bound states in other host materials in Figure 3a, which can be computed by density functional perturbation theory (DFPT). Our results in Figure 3b imply that applying cooling to the host materials can improve the lifetime of bound neutron states to a value close to the T^* shown in Figure 3a.

Quantum Control. It is also interesting to explore methods to control the transition between the neutronic ground and excited states. The neutronic states have weak coupling to external electromagnetic fields due to the charge neutrality of neutrons. Although such a weak coupling makes it difficult to apply direct microwave control protocols to transition between different neutronic states, we propose methods to manipulate the states through indirect coupling. As the neutron bound states are sensitive to the nuclide positions, which in turn are sensitive to electromagnetic waves if the QD is charged, they can be indirectly controlled by microwave driving. We take the LiH nanocrystal 1s and 1p neutronic states in Figure 1d as an example to illustrate allowed dipole transition, as they can be used as the two states of a qubit controlled by microwave. The direct Zeeman interaction of a neutron spin with the microwave's magnetic field is as weak as 10 kHz under a typical experimental condition with $B \sim 10$ G

https://doi.org/10.1021/acsnano.3c12929
ACS Nano 2024, 18, 9063−9070

(for example, a 10 G magnetic field shown in ref 39). The corresponding Rabi oscillation time period is as long as the lifetime of the bound neutron states, making microwave control through the magnetic field difficult. To achieve a strong driving, we instead propose to use an electric field, as shown in Figure 4a. The nanocrystal is electrostatically charged by the standard charging methods,[40,41] i.e., tuning the redox voltage so the net number of electrons does not balance the net nuclear charge, to a voltage of the order of magnitude of 1 V. The electric field of the microwave would then drive an oscillatory translation of the nanocrystal with net monopolar charge $q \neq 0$ and mass M, as in a driven oscillator model (off-resonance).[42] Since the neutronic state is aware of the translation of the center-of-mass of the nanoparticle, this controls the time-dependent Hamiltonian for the neutron parametrically and thus can drive the Rabi oscillation of a neutron between two bound states.

The Rabi frequency of a neutron between bound state i and j is (see SI, section S5 for derivation):

$$\Omega_{ij} = \frac{qm_n}{M\hbar}\frac{\omega_{ij}}{\omega}\vec{E}\cdot\int\overline{\psi}_i^*(\vec{r})\vec{r}\overline{\psi}_j(\vec{r})\mathrm{d}V \tag{8}$$

where ω and ω_{ij} are the microwave frequency and resonance frequency of the transition, $\vec{E}$ is the electric amplitude vector of the microwave. Initializing a neutron in the 1s state, the Rabi oscillation of the average neutron numbers in the 1s and 1p states is shown in Figure 4b. The Rabi oscillation is 2−3 orders of magnitude faster than its decay (here we only consider the decay from neutron absorption), allowing a pulse sequence of microwave control applied to the neutron qubit. Each pair of bound states following the selection rule of electric dipole transition has a transition matrix element, and the Rabi frequencies are generally on the order of magnitude of MHz with typical electric field intensity in experiments of kV/cm (for example, ref 43 applies an electric field of 3 kV/cm, and ref 44 applies a stronger electric field up to 500 kV/cm), as shown in Figure 4c. The Rabi frequency has a negative relation with the nanocrystal radius, providing strong coupling between 1s and 1p states up to 5 MHz (Figure 4d).

The above-studied neutron bound-state to bound-state transitions are mediated by microwave coupling to the mass of a charged quantum dot (the neutron does not couple directly to an electric field but is coupled to the nuclide mass distribution of the quantum dot). It is also possible to excite a neutron bound-state to an unbound continuum scattering state by microwave irradiation, using the same principle. The ability to "launch" bound neutrons to a specific momentum state controlled by the microwave frequency, polarization, and detailed morphology of the quantum dot is potentially useful for precision control of individual neutrons.

CONCLUSIONS

In this work, we demonstrated with analytical derivations and numerical calculations that hydride nanoparticles can host neutron bound states with ∼μeV binding energy, tens of nanometers extent, and ∼ms lifetime. The weakly bound neutron state can be controlled by the electric field of a microwave with a Rabi frequency of ∼MHz, to explore other bound excited states. To trap neutrons into μeV bound states in experiments, the incident neutrons need to be cooled to milli-Kelvin temperature, which can be realized by the ultracold neutron (UCN) source.[37] Although the neutron kinetic energy needs to be cooled to milli-Kelvin temperature, the nanoparticle material can have a much higher temperature (liquid-nitrogen temperature, Figure 3b) without significantly affecting the neutron bound states' lifetime, thanks to the slow energy transfer process between the host material and neutron through inelastic phonon scattering. The nuclear spins of hydrogens in the nanoparticles need to be polarized, which can be realized by DNP.

The NQD in a UCN bottle can be initialized to its ground state using a microwave with a frequency higher than the 1p state binding energy but lower than the 1s state binding energy. The microwave can deplete the neutron in excited states, and the ground-state NQDs will accumulate. The population of NQDs in different molecular neutronic states can be read out by the same microwave pulse and counting the outgoing neutrons. This gives the population of neutrons in the excited states. The tens of nanometers spatial extent of the neutron bound states provides possibilities to have multiqubit interaction. In comparison to the long-range electromagnetic interactions in Rydberg atom platforms generated by electrical dipole−dipole interactions,[45] the effective interactions between two quantum particles in NQDs are generated by the wave function overlap. The system we propose with feasible state preparation and control can be applied to explore fundamental physics such as characterizing the strong nuclear interaction with high precision and exploring the quantum statistics of different particles as well as develop certain quantum information processing applications.

METHODS

In order to prove the existence of molecular neutronic states, we need to show that the equations have nonzero solutions $\overline{\psi}_i$ with positive κ. In general cases, this can be solved only numerically. Here, we first provide a simplified model that shows the existence of molecular neutronic states analytically and then provide the computational workflow to solve the equation in general.

Assuming there are nuclei on an infinite cubic lattice with a lattice constant a, and each nucleus has a scattering length of b. We assume $\mathrm{Re}[b] \ll a$. Because of the periodicity of the lattice, the neutron eigenfunction follows the Bloch theorem. We consider the Bloch function at the Γ point, which means $\overline{\psi}_i$ on lattice points is a constant in the whole space. Then eq 4 gives

$$1 + \frac{\mathrm{Re}[b]}{a}\sum_{(x_1,x_2,x_3)\neq(0,0,0)}\frac{e^{-\kappa a\sqrt{x_1^2+x_2^2+x_3^2}}}{\sqrt{x_1^2+x_2^2+x_3^2}} = 0 \tag{9}$$

where (x_1, x_2, x_3) go through all combinations of integers except (0,0,0). We can easily see that the equation has a solution only when $\mathrm{Re}[b] < 0$. As $\frac{|\mathrm{Re}[b]|}{a} \ll 1$ and each term in the summation is less than 1, there must be a large number of lattice points contributing to the summation so that the second term can equal −1. That means the lattice is dense, and the summation can be approximated as an integral over the whole space:

$$1 + \frac{\mathrm{Re}[b]}{a}\int \mathrm{d}x^3\frac{e^{-\kappa a|x|}}{|x|} = 0 \tag{10}$$

The integral can be done analytically, giving $\frac{4\pi}{\kappa^2 a^2}$. The solution of the binding energy is then

$$E_b^* = \frac{\hbar^2\kappa^2}{2m_n} = -\frac{2\pi\hbar^2\mathrm{Re}[b]}{m_n a^3} \tag{11}$$

Similarly, if a unit cell contains multiple nuclei in an infinite crystal, the condition that allows this equation to have a solution is $\sum_\alpha n_\alpha \mathrm{Re}[b_\alpha] < 0$, where n_a and b_a are the number and scattering

https://doi.org/10.1021/acsnano.3c12929
ACS Nano 2024, 18, 9063−9070

length of the αth type of nucleus in a unit cell. The solution of the binding energy is then

$$E_b^* = \frac{\hbar^2\kappa^2}{2m_n} = -\frac{2\pi\hbar^2\sum_\alpha n_\alpha \mathrm{Re}[b_\alpha]}{m_n V_{\mathrm{u.c.}}} \tag{12}$$

which is eq 5 ($V_{\mathrm{u.c.}}$ is the unit cell volume). The order of magnitude of E_b, considering hydrogen-storage materials, is 0.1−1 μeV. The dispersion relation can also be obtained as

$$E(k) = \frac{\hbar^2}{2m_n}\left(\frac{4\pi\sum_\alpha n_\alpha \mathrm{Re}[b_\alpha]}{V_{\mathrm{u.c.}}} + k^2\right) \tag{13}$$

Using this equation, we can evaluate the mass gain of the LiH crystal when trapping neutrons. The Brillouin zone volume with $E(k) < 0$ is $V_{\mathrm{B.Z.}} = \frac{4\pi}{3}\left(-\frac{4\pi\sum_\alpha n_\alpha \mathrm{Re}[b_\alpha]}{V_{\mathrm{u.c.}}}\right)^{3/2}$. Assuming the neutron−neutron interaction in the molecular neutronic states is negligible, the neutron mass density in the material is $\rho_n = \frac{m_n V_{\mathrm{B.Z.}}}{(2\pi)^3}$. Then, the percentage mass gain discussed in the main text is

$$\frac{\rho_n}{\rho_{\mathrm{LiH}}} = \frac{4m_n}{3\sqrt{\pi}\rho_{\mathrm{LiH}}}\left(-\frac{\sum_\alpha n_\alpha \mathrm{Re}[b_\alpha]}{V_{\mathrm{u.c.}}}\right)^{3/2} \times 100\% \tag{14}$$

Using the data of the LiH crystal $\rho_{\mathrm{LiH}} = 780\ \mathrm{kg/m^3}$, $n_{\mathrm{Li}} = n_{\mathrm{H}} = 4$, $\mathrm{Re}[b_{\mathrm{Li}}] = -2.22$ fm (^{7}Li, unpolarized), $\mathrm{Re}[b_{\mathrm{H}}] = -18.33$ fm (^{1}H, fully polarized), $V_{\mathrm{u.c.}} = 68.09\ \mathrm{Å}^3$, $m_n = 1.675 \times 10^{-27}$ kg), we get a mass gain of 6.78×10^{-6}% for infinite 3D crystal of LiH.

As an infinite crystal can host bound neutronic states, we can conclude that a finite NQD can also host such states, as long as its size is sufficiently large. Then, we aim to numerically solve the molecular neutronic states for finite-size NQD. In order to obtain a manageable numerical problem, we do a coarse-graining by turning eq 4 into an integral equation using again the continuum approximation:

$$\bar{\psi}(\vec{r}) + \int_{\Omega_{\mathrm{n.c.}}} \mathrm{d}r'^3 \frac{e^{-\kappa|\vec{r}-\vec{r}'|}}{|\vec{r}-\vec{r}'|}\frac{\sum_\alpha n_\alpha \mathrm{Re}[b_\alpha]}{V_{\mathrm{u.c.}}}\bar{\psi}(\vec{r}') = 0 \tag{15}$$

where $\Omega_{\mathrm{n.c.}}$ is the nanocrystal region. The equation is then discretized by the coarse grid lattice $\vec{r}_i = (x_i, y_i, z_i)a_0$ with integer numbers of x_i, y_i, z_i. Then, the equation turns into:

$$\bar{\psi}(\vec{r}_i) + \frac{a_0^3\sum_\alpha n_\alpha \mathrm{Re}[b_\alpha]}{V_{\mathrm{u.c.}}}\sum_{j\neq i}\frac{e^{-\kappa r_{ij}}}{r_{ij}}\bar{\psi}(\vec{r}_j) = 0 \tag{16}$$

where $r_{ij} = |\vec{r}_i - \vec{r}_j|$, and grid separation a_0 is set as $R/10$, one tenth of the nanocrystal radius. All grid points within the nanocrystal sphere are included in eq 16 and are solved as an eigenvalue problem with eigenvector $(\bar{\psi}(\vec{r}_1), \bar{\psi}(\vec{r}_2), \ldots)$. Our numerical test shows that this a_0 gives good numerical convergence of binding energy to three effective digits accuracy.

ASSOCIATED CONTENT

Supporting Information

The Supporting Information is available free of charge at https://pubs.acs.org/doi/10.1021/acsnano.3c12929.

Detailed derivation of the neutron bound states formalism, derivation of the neutron absorption lifetime, details on materials screening shown in Figure 3a, derivation of neutron upscattering rate and details on the related DFT calculations, discussion about neutron bound states under incomplete nuclear spin polarization, derivation of the equation of motion, and Rabi frequency of microwave control (PDF)

AUTHOR INFORMATION

Corresponding Author

Ju Li − *Department of Materials Science and Engineering, Massachusetts Institute of Technology, Cambridge, Massachusetts 02139, United States; Department of Nuclear Science and Engineering, Massachusetts Institute of Technology, Cambridge, Massachusetts 02139, United States;* orcid.org/0000-0002-7841-8058; Email: liju@mit.edu

Authors

Hao Tang − *Department of Materials Science and Engineering, Massachusetts Institute of Technology, Cambridge, Massachusetts 02139, United States*

Guoqing Wang − *Research Laboratory of Electronics, Department of Nuclear Science and Engineering, and Department of Physics, Massachusetts Institute of Technology, Cambridge, Massachusetts 02139, United States;* orcid.org/0000-0002-1822-8121

Paola Cappellaro − *Research Laboratory of Electronics, Department of Nuclear Science and Engineering, and Department of Physics, Massachusetts Institute of Technology, Cambridge, Massachusetts 02139, United States;* orcid.org/0000-0003-3207-594X

Complete contact information is available at: https://pubs.acs.org/10.1021/acsnano.3c12929

Notes

The authors declare no competing financial interest.

ACKNOWLEDGMENTS

We thank Boning Li and Haowei Xu for their insightful discussion. This work was supported by the Office of Naval Research Multidisciplinary University Research Initiative Award No. ONR N00014-18-1-2497 and DTRA (Award No. HDTRA1-20-2-0002) Interaction of Ionizing Radiation with Matter (IIRM) University Research Alliance (URA). The preprint version of this work is available as Hao Tang; Guoqing Wang; Paola Cappellaro; Ju Li. μeV-deep neutron bound states in nanocrystals. 2023, 2309.07100, arXiv. https://arxiv.org/abs/2309.07100 (Accessed Feb. 8, 2024).

REFERENCES

(1) Willis, B. T. M.; Carlile, C. J. *Experimental Neutron Scattering*; Oxford University Press, 2017.

(2) Shirane, G. Neutron Scattering Studies of Structural Phase Transitions at Brookhaven. *Rev. Mod. Phys.* **1974**, *46* (3), 437.

(3) Muhlbauer, S.; Honecker, D.; Perigo, E. A.; Bergner, F.; Disch, S.; Heinemann, A.; Erokhin, S.; Berkov, D.; Leighton, C.; Eskildsen, M. R.; Michels, A. Magnetic Small-Angle Neutron Scattering. *Rev. Mod. Phys.* **2019**, *91* (1), 15004.

(4) Gabel, F.; Bicout, D.; Lehnert, U.; Tehei, M.; Weik, M.; Zaccai, G. Protein Dynamics Studied by Neutron Scattering. *Q. Rev. Biophys.* **2002**, *35* (4), 327−367.

(5) Schooneveld, E. M.; Pietropaolo, A.; Andreani, C.; Cippo, E. P.; Rhodes, N. J.; Senesi, R.; Tardocchi, M.; Gorini, G. Radiative Neutron Capture as a Counting Technique at Pulsed Spallation Neutron Sources: A Review of Current Progress. *Rep. Prog. Phys.* **2016**, *79* (9), 094301.

(6) Garcon, M.; Van Orden, J. W. The Deuteron: Structure and Form Factors. *Advances in Nuclear Physics*; Springer, 2001; pp 293−378.

(7) Geltman, S. Bound States in Delta Function Potentials. *J. At. Mol. Phys.* **2011**, *2011*, 1.

(8) Epelbaum, E.; Hammer, H.-W.; Meißner, U.-G. Modern Theory of Nuclear Forces. *Rev. Mod. Phys.* **2009**, *81* (4), 1773.
(9) Krane, K. S. *Introductory Nuclear Physics*; John Wiley & Sons, 1991.
(10) Hehre, W. J. Ab Initio Molecular Orbital Theory. *Acc. Chem. Res.* **1976**, *9* (11), 399−406.
(11) Sears, V. F. Neutron Scattering Lengths and Cross Sections. *Neutron news* **1992**, *3* (3), 26−37.
(12) Martin, J. W. Current Status of Neutron Electric Dipole Moment Experiments. In *Journal of Physics: Conference Series*; IOP Publishing, 2020; Vol. *1643*, p 12002.
(13) Abel, C.; Afach, S.; Ayres, N. J.; Baker, C. A.; Ban, G.; Bison, G.; Bodek, K.; Bondar, V.; Burghoff, M.; Chanel, E.; et al. Measurement of the Permanent Electric Dipole Moment of the Neutron. *Phys. Rev. Lett.* **2020**, *124* (8), 81803.
(14) Faber, M.; Ivanov, A. N.; Ivanova, V. A.; Marton, J.; Pitschmann, M.; Serebrov, A. P.; Troitskaya, N. I.; Wellenzohn, M. Continuum-State and Bound-State B–Decay Rates of the Neutron. *Phys. Rev. C* **2009**, *80* (3), 35503.
(15) Ashoori, R. C. Electrons in Artificial Atoms. *Nature* **1996**, *379* (6564), 413−419.
(16) Hou, T. Y. Numerical Approximations to Multiscale Solutions in Partial Differential Equations. *Frontiers in Numerical Analysis: Durham 2002* **2003**, 241−301.
(17) Gould, C. R.; Sharapov, E. I. Fermi's Favorite Figure: The History of the Pseudopotential Concept in Atomic Physics and Neutron Physics. *European Physical Journal H* **2022**, *47* (1), 10.
(18) Economou, E. N. *Green's Functions in Quantum Physics*; Springer Science & Business Media, 2006; Vol. *7*.
(19) Kresse, G.; Joubert, D. From Ultrasoft Pseudopotentials to the Projector Augmented-Wave Method. *Phys. Rev. B* **1999**, *59* (3), 1758−1775.
(20) Perdew, J. P.; Burke, K.; Ernzerhof, M. Generalized Gradient Approximation Made Simple. *Phys. Rev. Lett.* **1996**, *77* (18), 3865−3868.
(21) Kresse, G.; Furthmüller, J. Efficient Iterative Schemes for Ab Initio Total-Energy Calculations Using a Plane-Wave Basis Set. *Phys. Rev. B* **1996**, *54* (16), 11169−11186.
(22) Monkhorst, H. J.; Pack, J. D. Special Points for Brillouin-Zone Integrations. *Phys. Rev. B* **1976**, *13* (12), 5188−5192.
(23) Togo, A.; Tanaka, I. First Principles Phonon Calculations in Materials Science. *Scr Mater.* **2015**, *108*, 1−5.
(24) Corzilius, B. High-Field Dynamic Nuclear Polarization. *Annu. Rev. Phys. Chem.* **2020**, *71*, 143−170.
(25) Roinel, Y.; Bouffard, V. Polarisation Dynamique Nucléaire Dans l'hydrure de Lithium. *J. Phys. (Paris)* **1977**, *38* (7), 817−824.
(26) Imamoglu, A.; Knill, E.; Tian, L.; Zoller, P. Optical Pumping of Quantum-Dot Nuclear Spins. *Phys. Rev. Lett.* **2003**, *91* (1), 17402.
(27) Banger, S.; Nayak, V.; Verma, U. P. Hydrogen Storage in Lithium Hydride: A Theoretical Approach. *J. Phys. Chem. Solids* **2018**, *115*, 6−17.
(28) Niemann, M. U.; Srinivasan, S. S.; Phani, A. R.; Kumar, A.; Goswami, D. Y.; Stefanakos, E. K. Nanomaterials for Hydrogen Storage Applications: A Review. *J. Nanomater.* **2008**, *2008*, 1.
(29) Napan, R.; Peltzer y Blancá, E. L. First-Principles Studies of Lithium Hydride Series for Hydrogen Storage. *Int. J. Hydrogen Energy* **2012**, *37* (7), 5784−5789.
(30) Wang, L.; Quadir, M. Z.; Aguey-Zinsou, K.-F. Ni Coated LiH Nanoparticles for Reversible Hydrogen Storage. *Int. J. Hydrogen Energy* **2016**, *41* (15), 6376−6386.
(31) Bramwell, P. L.; Ngene, P.; de Jongh, P. E. Carbon Supported Lithium Hydride Nanoparticles: Impact of Preparation Conditions on Particle Size and Hydrogen Sorption. *Int. J. Hydrogen Energy* **2017**, *42* (8), 5188−5198.
(32) Griffith, J. S.; Orgel, L. E. Ligand-Field Theory. *Quarterly Reviews, Chemical Society* **1957**, *11* (4), 381−393.
(33) Weber, E. *Spatial and Temporal Evolution of Dynamic Nuclear Polarization on Different Scales*; Université Paris Sciences et Lettres, 2021.
(34) Adair, R. K. Neutron Cross Sections of the Elements. *Rev. Mod. Phys.* **1950**, *22* (3), 249.
(35) Liu, C.-Y.; Young, A. R.; Lamoreaux, S. K. Ultracold Neutron Upscattering Rates in a Molecular Deuterium Crystal. *Phys. Rev. B* **2000**, *62* (6), R3581−R3583.
(36) Jain, A.; Ong, S. P.; Hautier, G.; Chen, W.; Richards, W. D.; Dacek, S.; Cholia, S.; Gunter, D.; Skinner, D.; Ceder, G.; Persson, K. A. Commentary: The Materials Project: A Materials Genome Approach to Accelerating Materials Innovation. *APL Mater.* **2013**, *1* (1), na.
(37) Bison, G.; Daum, M.; Kirch, K.; Lauss, B.; Ries, D.; Schmidt-Wellenburg, P.; Zsigmond, G.; Brenner, T.; Geltenbort, P.; Jenke, T.; et al. Comparison of Ultracold Neutron Sources for Fundamental Physics Measurements. *Phys. Rev. C* **2017**, *95* (4), 45503.
(38) Pardalos, P. M.; Migdalas, A.; Pitsoulis, L. *Pareto Optimality, Game Theory and Equilibria*; Springer Science & Business Media, 2008; Vol. *17*.
(39) Wang, G.; Liu, Y.-X.; Zhu, Y.; Cappellaro, P. Nanoscale Vector AC Magnetometry with a Single Nitrogen-Vacancy Center in Diamond. *Nano Lett.* **2021**, *21* (12), 5143−5150.
(40) Abbas, Z.; Labbez, C.; Nordholm, S.; Ahlberg, E. Size-Dependent Surface Charging of Nanoparticles. *J. Phys. Chem. C* **2008**, *112* (15), 5715−5723.
(41) Frimmer, M.; Luszcz, K.; Ferreiro, S.; Jain, V.; Hebestreit, E.; Novotny, L. Controlling the Net Charge on a Nanoparticle Optically Levitated in Vacuum. *Phys. Rev. A* **2017**, *95* (6), 61801.
(42) Hempston, D.; Vovrosh, J.; Toroš, M.; Winstone, G.; Rashid, M.; Ulbricht, H. Force Sensing with an Optically Levitated Charged Nanoparticle. *Appl. Phys. Lett.* **2017**, *111* (13), na.
(43) Dolde, F.; Fedder, H.; Doherty, M. W.; Nobauer, T.; Rempp, F.; Balasubramanian, G.; Wolf, T.; Reinhard, F.; Hollenberg, L. C. L.; Jelezko, F.; Wrachtrup, J. Electric-Field Sensing Using Single Diamond Spins. *Nat. Phys.* **2011**, *7* (6), 459−463.
(44) Bennett, A. J.; Pooley, M. A.; Cao, Y.; Sköld, N.; Farrer, I.; Ritchie, D. A.; Shields, A. J. Voltage Tunability of Single-Spin States in a Quantum Dot. *Nat. Commun.* **2013**, *4* (1), 1522.
(45) Saffman, M.; Walker, T. G.; Mølmer, K. Quantum Information with Rydberg Atoms. *Rev. Mod. Phys.* **2010**, *82* (3), 2313.

https://doi.org/10.1021/acsnano.3c12929
ACS Nano 2024, 18, 9063−9070

Supporting Information: μeV-deep neutron bound states in nanocrystals

Hao Tang,[1] Guoqing Wang,[2,3] Paola Cappellaro,[2,3,4] and Ju Li[1,3,*]

[1]*Department of Materials Science and Engineering, Massachusetts Institute of Technology, MA 02139, USA*
[2]*Research Laboratory of Electronics, Massachusetts Institute of Technology, Cambridge, MA 02139, USA*
[3]*Department of Nuclear Science and Engineering, Massachusetts Institute of Technology, Cambridge, MA 02139, USA*
[4]*Department of Physics, Massachusetts Institute of Technology, Cambridge, MA 02139, USA*

(Dated: February 21, 2024)

S1. NEUTRON BOUND STATES

Here we describe the formalism of neutrons' low energy bound states in a nuclear force potential created by multiple nuclei. The Hamiltonian of the system is

$$H = -\frac{\hbar^2}{2m_n}\nabla^2 + \sum_i v_i(\vec{r}), \tag{S1}$$

where $v_i(\vec{r})$ is the nuclear force potential energy of the ith nucleus to a neutron. Here, we employ the Green function formalism. The time-independent Schrodinger equation for an energy eigenfunction $\psi(\vec{r})$ can be written as:

$$\left[-\frac{\hbar^2}{2m_\mathrm{n}}\nabla^2 + V(\vec{r})\right]\psi(\vec{r}) = E\psi(\vec{r}) = -\frac{\hbar^2\kappa^2}{2m_\mathrm{n}}\psi(\vec{r}), \tag{S2}$$

where we define $V(\vec{r}) \equiv \sum_i v_i(\vec{r})$ the wave vector $\kappa \equiv \frac{\sqrt{-2m_nE}}{\hbar}$ for bound states. The above equation is equivalent to:

$$\left(\kappa^2 - \nabla^2\right)\psi(\vec{r}) = -\frac{2m_\mathrm{n}V(\vec{r})}{\hbar^2}\psi(\vec{r}). \tag{S3}$$

The Green function of this equation satisfies:

$$\begin{cases}\left(\kappa^2 - \nabla^2\right)G(\vec{r},\vec{r}';E) = \delta(\vec{r}-\vec{r}') \\ \lim_{|\vec{r}-\vec{r}'|\to\infty} G(\vec{r},\vec{r}';E) = 0,\end{cases} \tag{S4}$$

which gives

$$G(\vec{r},\vec{r}';E) = \frac{e^{-\kappa|\vec{r}-\vec{r}'|}}{4\pi|\vec{r}-\vec{r}'|}. \tag{S5}$$

The energy eigenfunctions can then be formally expressed as:

$$\psi(\vec{r}) = -\int G(\vec{r},\vec{r}';E)\frac{2m_\mathrm{n}V(\vec{r}')}{\hbar^2}\psi(\vec{r}')dr'^3, \tag{S6}$$

which is Eq. (1) in the main text. The integral can be rewritten as a sum of local integrals around each nucleus:

$$\psi(\vec{r}) = -\sum_i \int_{\Omega_i} G(\vec{r},\vec{r}';E)\frac{2m_\mathrm{n}v_i(\vec{r}')}{\hbar^2}\psi(\vec{r}')dr'^3, \tag{S7}$$

where Ω_i is a spherical volume around the ith nucleus with a radius of the nuclear force range. We consider two cases: the first is $\vec{r}$ is not fm-scale close to any nuclei. As G is a slowly varying function of $\vec{r}'$ that is approximately a constant at each nucleus' fm-scale neighborhood, it can be taken out of the integral, replacing $\vec{r}'$ by $\vec{R}_i$ (case 1 of main text Eq. (2)):

$$\psi(\vec{r}) = -\sum_i G(\vec{r},\vec{R}_i;E)\int_{\Omega_i}\frac{2m_\mathrm{n}v_i(\vec{r}')}{\hbar^2}\psi(\vec{r}')dr'^3. \tag{S8}$$

The second case is that $\vec{r}$ is ∼fm close to the jth nucleus, so extracting G out of the integral around Ω_j in Eq. (S8) is invalid. Then we need to add a contribution from the jth nucleus' neighborhood (case 2 of main text Eq.(2)):

$$\begin{aligned}\psi(\vec{r}) = &-\sum_{i\neq j} G(\vec{r},\vec{R}_i;E)\int_{\Omega_i}\frac{2m_\mathrm{n}v_i(\vec{r}')}{\hbar^2}\psi(\vec{r}')dr'^3 \\ &-\int_{\Omega_j} G(\vec{r},\vec{r}';E)\frac{2m_\mathrm{n}v_j(\vec{r}')}{\hbar^2}\psi(\vec{r}')dr'^3.\end{aligned} \tag{S9}$$

As we consider the low-energy case, this integral can then be simplified following the typical assumptions of the Fermi pseudopotential. We can introduce the scattering length, b_i, for low-energy neutron [1] whose real part is $\mathrm{Re}[b_i] \equiv \lim_{E\to 0}\frac{1}{4\pi\bar{\psi}(\vec{R}_i)}\int_{\Omega_i}\frac{2m_nv_i(\vec{r}')}{\hbar^2}\psi(\vec{r}')dr'^3$, where $\bar{\psi}(\vec{r})$ is the average eigenfunction [1]:

$$\bar{\psi}(\vec{r}) = \frac{3}{4\pi D^3}\int_{|\vec{r}-\vec{r}'|<D}\psi(\vec{r}')dr'^3. \tag{S10}$$

Here D is a length that is far smaller than the interatomic distance but far larger than the force range of nuclear potential. This approximation can be taken because the interatomic distance is five orders of magnitude large than the force range of nuclear force. Eq. (S8) and Eq. (S9) can be simplified using the average eigenfunction and scattering length. The first case (Eq. (S8)) gives:

$$\begin{aligned}\bar{\psi}(\vec{r}) \simeq \psi(\vec{r}) &= -4\pi\sum_i G(\vec{r},\vec{R}_i;E)\mathrm{Re}[b_i]\bar{\psi}(\vec{R}_i) \\ &= -\sum_i \frac{e^{-\kappa|\vec{r}-\vec{R}_i|}}{|\vec{r}-\vec{R}_i|}\mathrm{Re}[b_i]\bar{\psi}(\vec{R}_i), \quad \forall i(|\vec{r}-\vec{R}_i| \gg \mathrm{fm}),\end{aligned} \tag{S11}$$

* liju@mit.edu

where $\bar{\psi}(\vec{r})$ approximately equals $\psi(\vec{r})$ as the later is slowly varying at the length-scale D when $\vec{r}$ is far from nuclei. The second case (Eq. (S9)) gives:

$$\psi(\vec{r}) = -\sum_{i\neq j}\frac{e^{-\kappa|\vec{r}-\vec{R}_i|}}{|\vec{r}-\vec{R}_i|}\mathrm{Re}[b_i]\bar{\psi}(\vec{R}_i) - \int_{\Omega_j}\frac{e^{-\kappa|\vec{r}-\vec{r}'|}}{|\vec{r}-\vec{r}'|}\frac{m_\mathrm{n}v_j(\vec{r}')}{2\pi\hbar^2}\psi(\vec{r}')dr'^3, (|\vec{r}-\vec{R}_j|\sim \mathrm{fm}). \tag{S12}$$

The average eigenfunction around the nuclei can be derived by substituting this equation into Eq. (S10). Using the slow varying condition again for the first term, we obtain

$$\bar{\psi}(\vec{r}) = -\sum_{i\neq j}\frac{e^{-\kappa|\vec{r}-\vec{R}_i|}}{|\vec{r}-\vec{R}_i|}\mathrm{Re}[b_i]\bar{\psi}(\vec{R}_i) - \frac{3}{4\pi D^3} \times \int_{|\vec{r}_1-\vec{r}|<D} dr_1^3\int_{\Omega_j} dr_2^3\frac{e^{-\kappa|\vec{r}_1-\vec{r}_2|}}{|\vec{r}_1-\vec{r}_2|}\frac{m_\mathrm{n}v_j(\vec{r}_2)\psi(\vec{r}_2)}{2\pi\hbar^2}. \tag{S13}$$

In the second term, we can first do the integral $\int_{|\vec{r}_1-\vec{r}|<D}\frac{e^{-\kappa|\vec{r}_1-\vec{r}_2|}}{|\vec{r}_1-\vec{r}_2|}dr_1^3$, and as $\kappa D \ll 1$, the exponential term in the Green function approximates 1. As both $\vec{r}$ and $\vec{r}_2$ are fm-close to $\vec{R}_j$, their distance is also in fm scale, far smaller than D. The integral gives $2\pi D^2$, then the second term equals $-\frac{3}{2D}\mathrm{Re}[b_j]\bar{\psi}(\vec{R}_j)$. As $D \gg$ fm, this term is negligible compared to $\bar{\psi}$ itself, so only the first term remains. Summarizing the two cases gives the general expression of the average eigenfunction:

$$\bar{\psi}(\vec{r}) \simeq -\sum_{i,|\vec{r}-\vec{R}_i|\gg\mathrm{fm}}\frac{e^{-\kappa\left|\vec{r}-\vec{R}_i\right|}}{\left|\vec{r}-\vec{R}_i\right|}\mathrm{Re}[b_i]\bar{\psi}\left(\vec{R}_i\right), \tag{S14}$$

which is Eq. (3) in the main text. To get a closed set of equations, we set $\vec{r}=\vec{R}_i$ and denote $\bar{\psi}\left(\vec{R}_i\right)$ as $\bar{\psi}_i$:

$$\bar{\psi}_i + \sum_{j\neq i}\frac{e^{-\kappa\left|\vec{R}_i-\vec{R}_j\right|}}{\left|\vec{R}_i-\vec{R}_j\right|}\mathrm{Re}[b_j]\bar{\psi}_j = 0, \tag{S15}$$

which is Eq. (4) in the main text.

Finally, we reexamine the applicability of Fermi pseudopotential in molecular neutronic states. Here, we prove that $\lim_{E\to 0}\frac{1}{4\pi\bar{\psi}(\vec{R}_i)}\int_{\Omega_i}\frac{2m_n v_i(\vec{r}')}{\hbar^2}\psi(\vec{r}')dr'^3$ converges to the same number regardless of whether E approaches zero from a positive or negative direction. That validates our usage of the scattering length from neutron scattering data to molecular neutronic states. As the force range of $v_i(\vec{r})$ is far smaller than $1/\kappa$, the eigenfunction near a nucleus is accurately approximated as an s-wave. We denote the wave function around R_i as $\psi(r)$ and $u(r)\equiv r\psi(r)$, where r is the distance from the nucleus. The eigenvalue equation is:

$$-\frac{\hbar^2}{2m_n}\frac{d^2u}{dr^2} + v_i(r)u(r) = Eu(r). \tag{S16}$$

At r larger than the force range R_0, the potential $v_i(r)=0$, then we have $u''(r)=0$ given $E\to 0$. That means the $u(r)|_{r>R_0} = k(r+c_0)$ is a linear function. The average eigenfunction $\bar{\psi}_i = \frac{3}{4\pi D^3}\int_0^D u(r)4\pi r dr \simeq k$ (as $c_0, R_0 \ll D$). We can then integrate Eq. (S16) multiplied by r from $r=0$ to $r=R_0$:

$$-\frac{\hbar^2}{2m_n}\int_0^{R_0}dr\frac{d^2u}{dr^2}r + \int_0^{R_0}v_i(r)u(r)rdr = 0. \tag{S17}$$

That gives:

$$-\frac{\hbar^2}{2m_n}\left[r\frac{du}{dr}-u(r)\right]_0^{R_0} + \frac{1}{4\pi}\int_{\Omega_i}v_i(\vec{r})\psi(\vec{r})dr = 0. \tag{S18}$$

As $u(0)=0, R_0\frac{du}{dr}|_{R_0} - u(R_0) = -kc_0$, we obtain

$$\frac{\hbar^2}{2m_n}c_0\bar{\psi}_i + \frac{1}{4\pi}\int_{\Omega_i}v_i(\vec{r})\psi(\vec{r})dr^3 = 0. \tag{S19}$$

That proves the expression $\frac{1}{4\pi\bar{\psi}(\vec{R}_i)}\int_{\Omega_i}\frac{2m_n v_i(\vec{r}')}{\hbar^2}\psi(\vec{r}')dr'^3$ approaches a constant of $-c_0$, which is defined as $\mathrm{Re}[b_i]$, when E approaches zero. Here, neglecting the E-term applies as long as $\sqrt{2m_n|E|}/\hbar \ll \mathrm{fm}^{-1}$ regardless of the sign of E, so the low-energy scattering state and bound state have the same scattering length.

S2. NEUTRON ABSORPTION LIFETIME AND MATERIALS SCREENING

In addition to the binding energy, it is also important to evaluate other effects that might limit the lifetime of molecular neutronic states. In the Hamiltonian in Eq. (S1), we did not consider electromagnetic radiation, which leads to the radiative neutron absorption process where a neutron drops into a MeV deep bound state and emits a γ-ray photon. This neutron absorption process makes the neutron bound state unstable. The low-energy neutron absorption rate is proportional to the Fermi contact, with a constant of low-energy absorption cross-section $\sigma_a(E_k)$ multiplied by neutron velocity $\sqrt{2E_k/m_n}$ [2]. Summing over all nucleus, the absorption rate of a molecular neutronic state in a uniform perfect crystal is:

$$\frac{d\Gamma}{dt} = \frac{1}{T^*} = \sum_i|\bar{\psi}_i|^2\lim_{E_k\to 0}\sigma_a^i(E_k)\sqrt{\frac{2E_k}{m_n}} = \lim_{E_k\to 0}\frac{1}{V_{u.c.}}\sum_\alpha n_\alpha\sigma_a^\alpha(E_k)\sqrt{\frac{2E_k}{m_n}}, \tag{S20}$$

which is Eq. (5) in the main text. In the second line, we use the condition that $\bar{\psi}$ is normalized and constant in space.

If the nanocrystal has a finite size, the argument based on the uniform wave function is no longer valid. Interestingly, the product of binding energy and absorption rate

are upper bounded. The binding energy can be rewritten as the opposite of the summation of potential energy and kinetic energy:

$$E_b = -\frac{2\pi\hbar^2}{m_n}\sum_i \mathrm{Re}[b_i]|\bar{\psi}_i|^2 - \langle\hat{E}_k\rangle \le -\frac{2\pi\hbar^2}{m_n}\sum_i \mathrm{Re}[b_i]|\bar{\psi}_i|^2, \tag{S21}$$

where $\langle\hat{E}_k\rangle$ is the average kinetic energy, sum over i goes through all unit cells m and all the atom types α in each unit cell. As $\bar{\psi}$ is slowly varying in the scale of a unit cell, the inequality approximates:

$$E_b \le -\frac{2\pi\hbar^2}{m_n}\sum_m |\bar{\psi}_m|^2 \sum_\alpha n_\alpha \mathrm{Re}[b_\alpha], \tag{S22}$$

where $\bar{\psi}_m$ is the average eigenfunction in the mth unit cell. The absorption rate, by this notation, can be written as:

$$\frac{1}{T_{\mathrm{life}}} = \sum_m |\bar{\psi}_m|^2 \lim_{E_k\to 0}\sum_\alpha n_\alpha \sigma_a^\alpha(E_k)\sqrt{\frac{2E_k}{m_n}}. \tag{S23}$$

We therefore have

$$E_b T_{\mathrm{life}} \le -\frac{2\pi\hbar^2}{m_n}\frac{\sum_\alpha n_\alpha \mathrm{Re}[b_\alpha]}{\lim_{\alpha\to 0}\sum_\alpha n_\alpha \sigma_a^\alpha(E_k)\sqrt{\frac{2E_k}{m_n}}} = E_b^* T^*, \tag{S24}$$

which is Eq. (6) in the main text. It is worth noticing that the inequality can be transformed into an inspiring form, which is similar to the time-energy uncertainty principle. The low energy absorption cross section is related to the imaginary part of the scattering length [2]:

$$\sigma_a^\alpha(E_k) = \frac{4\pi\,\mathrm{Im}[b_\alpha]}{k} = 4\pi\,\mathrm{Im}[b_\alpha]\sqrt{\frac{\hbar^2}{2m_n E_k}}. \tag{S25}$$

Substituting this back into Eq. (S24), we derive

$$E_b T_{\mathrm{life}} \le -\frac{\hbar}{2}\frac{\sum_\alpha n_\alpha\,\mathrm{Re}[b_\alpha]}{\sum_\alpha n_\alpha\,\mathrm{Im}[b_\alpha]}. \tag{S26}$$

We see that compared to the time-energy uncertainty principle, the upper bound has an amplification of $\frac{\mathrm{Re}[b_\alpha]}{\mathrm{Im}[b_\alpha]}$, which is 10^6 for polarized hydrogen atoms.

In the materials screening, we select crystal structures from all available structures in the Materials project containing hydrogen. We first exclude structures not stable and structures containing elements heavier than La (because they generally have excessively high absorption cross sections and cannot give a reasonable lifetime), and then calculate E_b^* and T^* by Eq. (5) in the main text. The values of b_i are extracted from ref. [2], where we assume that H nuclei are fully polarized, and all other nuclei are non-polarized. For most elements, we assume a natural abundance of isotopes, except for a few elements: we assume Li, B, Cl, and Se are purified as ^{7}Li, ^{11}B, ^{37}Cl, ^{80}Se, because these isotopes are naturally abundant and the purification significantly improves lifetime in some compound.

S3. NEUTRON UPSCATTERING

In this section, we elaborate the derivation and computational details to obtain the neutron upscattering rate shown in Fig. 3b in the main text. The total Hamiltonian of the neutron phonon system is $\hat{H} = \hat{H}_{\mathrm{n}} + \hat{H}_{\mathrm{ph}} + \hat{V}_{\mathrm{int}}$, where $\hat{H}_n = -\frac{\hbar^2}{2m_{\mathrm{n}}}\nabla^2 + \sum_i v_i(\vec{r})$ is the neutron Hamiltonian when nuclei are at equilibrium positions, $H_{\mathrm{ph}} = \sum_j \hbar\omega_j(\hat{n}_j + \frac{1}{2})$ is the phonon Hamiltonian under harmonic approximation, and $\hat{V}_{\mathrm{int}} = -\sum_i \vec{Q}_i \cdot \nabla v_i(\vec{r})$ is the interaction between neutron and phonon expanded to the first-order of atomic displacement $\vec{Q}_i$. In the Hamiltonians, ω_j and $\hat{n}_j$ are the vibration frequency and phonon number operator of the jth vibration mode. The atomic displacement operator can be expressed as phonon creation and annihilation operators, $a_j^\dagger$ and a_j:

$$\vec{Q}_i = \sum_j \sqrt{\frac{\hbar}{2M_j\omega_j}}(a_j^\dagger + a_j)\vec{e}_{ij} \tag{S27}$$

where M_j and $\vec{e}_{ij}$ are the effective mass and polarization vector of the jth phonon mode. Assuming $\hat{V}_{\mathrm{int}}$ is a perturbation, the neutron upscattering rate can then be calculated using Fermi's golden rule.

Initially, we assume the neutron is at the lowest bound state $\psi_0(\vec{r})$ with energy E_0. The phonon is at thermal equilibrium, which has $P(\{n_j\}, T) = \prod_j \frac{1}{Z_j} e^{-n_j\hbar\omega_j/k_{\mathrm{B}}T}$ probability of being at state $|\{n_j\}\rangle$ with energy $E_{\{n_j\}}$(having n_j phonons at mode j. Z_j is the partition function). The final state of the neutron is $\psi_k(\vec{r}) = e^{i\vec{k}\cdot\vec{r}}$ with energy $E_k = \frac{\hbar^2k^2}{2m_n}$, and the final state of phonons is $|\{n_j'\}\rangle$ (with energy $E_{\{n_j'\}}$) where one phonon is absorbed. The total transition rate is then:

$$\Gamma_{\mathrm{upscattering}} = \frac{2\pi}{\hbar}\sum_{\{n_j\},\{n_j'\}}\int\frac{d^3k}{(2\pi)^3}P(\{n_j\},T)$$
$$|\langle\psi_k,\{n_j'\}|\hat{V}_{\mathrm{int}}|\psi_0,\{n_j\}\rangle|^2\delta(E_k + E_{\{n_j'\}} - E_0 - E_{\{n_j\}}) \tag{S28}$$

Substituting the expressions of $P(\{n_j\},T), \hat{V}_{\mathrm{int}}$, and all energy terms, the expression is simplified to:

$$\Gamma_{\mathrm{upscattering}} = \frac{2\pi}{\hbar}\sum_j\int\frac{d^3k}{(2\pi)^3}f_{\mathrm{B.E.}}(\omega_j,T)\frac{\hbar}{2M_j\omega_j}$$
$$|\sum_i \vec{e}_{ij}\cdot\langle\psi_k|\nabla v_i(\vec{r})|\psi_0\rangle|^2\delta(E_k - E_0 - \hbar\omega_j) \tag{S29}$$

Taking the bulk crystal limit for a nanoparticle, the summation over vibrational modes $\sum_j$ turns into $\sum_n\int\frac{d^3k'}{(2\pi)^3}$, M_j becomes $M_{nk}^{\mathrm{u.c.}}N_{\mathrm{u.c.}}$ (effective mass in one unit cell times the number of unit cells), and $\vec{e}_{ij}$ becomes $\sum_i \vec{e}^{\,0}_{i,nk'}e^{i\vec{k}'\cdot\vec{R}_i}$, where $\vec{e}^{\,0}_{i,nk'}$ is the polarization vector in one unit cell. Using the average wavefunction $\bar{\psi}_0 \simeq 1$ and Fermi pseudopotential $v_i(\vec{r}) = \frac{2\pi\hbar^2 b_i}{m_n}\delta(\vec{r} - \vec{R}_{i0})$ to

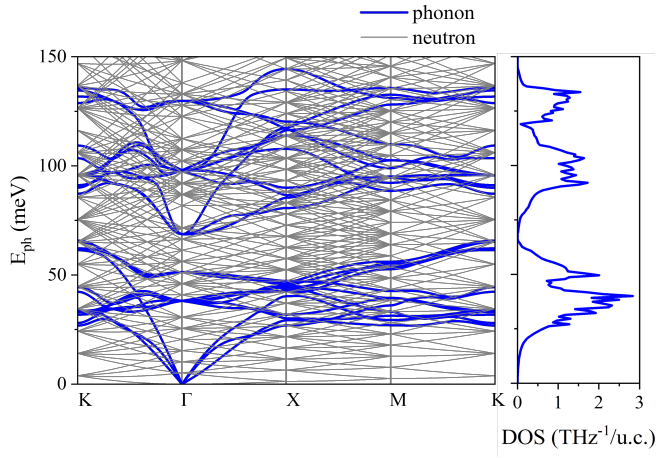

FIG. S1. Phonon band structure and density of states (blue lines) of LiH crystal calculated by the DFT. The grey lines are band structure of the final-state free neutrons.

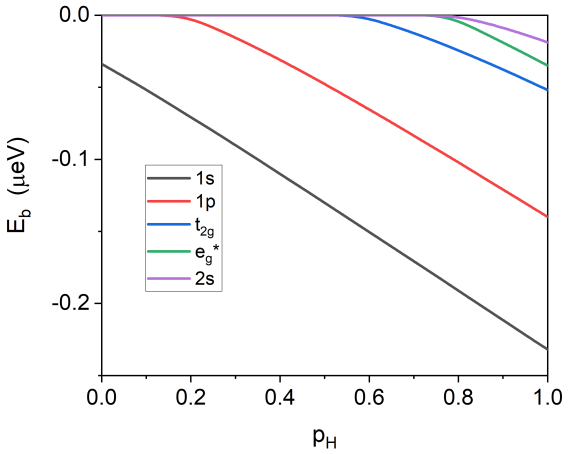

FIG. S2. Energy levels of the molecular neutronic states in 40 nm-radius spherical LiH nanoparticle with incomplete hydrogen nuclear spin polarization $p_{\rm H}$. We assume that $p_{\rm H}$ is uniform and constant in the nanoparticle.

evaluate the matrix element, we get

$$\langle\psi_k|\nabla v_i(\vec{r})|\psi_0\rangle = i\vec{k}\frac{2\pi\hbar^2}{m_n}b_i e^{-i\vec{k}\cdot\vec{r}} \tag{S30}$$

The $|\sum_i \vec{e}_{ij}\cdot\langle\psi_k|\nabla v_i(\vec{r})|\psi_0\rangle|^2$ then gives:

$$(2\pi)^3 N_{\rm u.c.}\Omega_{\rm u.c.}(\frac{2\pi\hbar^2}{m_n})^2\sum_m|\vec{k}\cdot\sum_{i\in{\rm u.c.}}\vec{e}^{\,0}_{i,nk'}b_i|^2\delta(\vec{k}-\vec{G}_m-\vec{k}') \tag{S31}$$

where $\Omega_{u.c.}$ is the unic cell volume and $\vec{G}_m$ is the inverse lattice vector (indexed by m). Summarizing these results together, we obtain

$$\Gamma_{\rm upscattering} = \frac{\hbar^4}{2m_n^2}\sum_n\int d^3k f_{\rm B.E.}(\omega_{nk},T)\frac{\Omega_{\rm u.c.}}{M^{\rm u.c.}_{nk}\omega_{nk}}$$
$$\sum_m|(\vec{k}+\vec{G}_m)\cdot\sum_{i\in{\rm u.c.}}\vec{e}^{\,0}_{i,nk}b_i|^2\delta(E_k-E_0-\hbar\omega_{nk}) \tag{S32}$$

which is Eq. (7) in the main text.

In order to evaluate Eq. (7) in the main text, we first conduct DFT calculations to evaluate the phonon band structures ω_{nk} and polarization vectors $\vec{e}^{\,0}_{i,nk}$. We use LiH crystal as an example. The DFT calculations are implemented by Vienna ab-initio simulation package (VASP) [3] using the projector-augmented wave (PAW) method [4]. The generalized gradient approximation (GGA) is employed with the Perdew-Burke-Ernzerhof (PBE) functional [5]. The k-point mesh is sampled by the Monkhorst-Pack method [6] with a separation of 0.2 rad/Å. Electronic iterations converge to 10^{-6} eV and forces in atomic relaxation converges to 0.01 eV/Å. The force constant matrix is calculated using density functional perturbation theory (DFPT) implemented in VASP using a $3\times3\times3$ supercell. The phonon band structure and polarization vectors are then calculated using the phonopy package [7] on a $50\times50\times50$ k-point mesh.

The calculated phonon band structure and density of states are plotted in Fig. S1. We evaluate the neutron up-scattering rate using Eq. (7) in the main text, where the integral over k is numerically evaluated on the $50\times50\times50$ k-point mesh, and the energy δ-function is smeared as a Gaussian function with $\sigma = 0.2h\times$THz. In the summation over inverse lattice vectors $\vec{G}_m = \sum_{l=1}^3 m_l\vec{b}_l$, m_1, m_2, m_3 goes through all integers in [-3, 3]. We examine that the calculated scattering rates are well convergent over all numerical parameters. The calculation gives results in Fig. 3b in the main text.

S4. IMPACT OF INCOMPLETE NUCLEAR SPIN POLARIZATION

Here we consider the case when the hydrogen nuclear spins are not fully polarized. The scattering length b_i is consists of a coherent part $b_{i,\rm coherent}$ and an incoherent part $b_{i,\rm incoherent}$:

$$b_i = b_{i,\rm coherent} + \frac{2b_{i,\rm incoherent}}{\sqrt{I(I+1)}}\vec{s}\cdot\vec{I}. \tag{S33}$$

Consider the density matrix of the nuclear spin ensemble is ρ_I. We define the polarization $\vec{p}_{\rm H} = \frac{1}{I}{\rm Tr}[\vec{I}\rho_I]$ oriented towards z-direction. Assuming the neutron spin is completely polarized in the opposite direction of the nuclear polarization, then we have $\vec{s} = -\frac{\vec{e}_z}{2}$ (as $I = 1/2$ for H). Then, the average scattering length in the nuclear spin ensemble is

$$\langle b_i\rangle = {\rm Tr}[b_i\rho] = b_{i,\rm coherent} - \frac{p_{\rm H}}{\sqrt{3}}b_{i,\rm incoherent}. \tag{S34}$$

Energy levels of molecular neutronic states are then evaluated by substituting the $\langle b_i\rangle$ in Eq. (S34)into Eq. (4) in

the main text, as shown in Fig. S2. The results verify that the molecular neutronic states is robust against slightly incomplete polarization. In the rest part of this paper, we assume $p_H = 1$,

S5. MICROWAVE CONTROL

The microwave applies an electric field on a charged nanocrystal with a mass of $M = \frac{4\pi}{3}R^3\rho$ and an electric charge of q. If the electric field is

$$\vec{E}(t) = \vec{E}_0 \sin \omega t. \tag{S35}$$

Then the coordinates $\vec{R}$ of the center of the charged nanocrystal is

$$\vec{R}(t) = -\frac{q\vec{E}_0}{M\omega^2} \sin \omega t. \tag{S36}$$

The time-dependent Schrodinger equation $\hat{H}_{\vec{R}(r)}\psi = i\hbar\frac{\partial\psi}{\partial t}$ gives:

$$c'_m(t) + \sum_n c_n(t)\vec{R}'(r)\cdot\langle\psi_{m,R(t)}|\nabla_R|\psi_{n,R(t)}\rangle = \frac{1}{i\hbar}c_m(t)E_m, \tag{S37}$$

where $c_m(t)$ is the wave function in the energy representation and Schrodinger picture: $|\psi(t)\rangle = \sum_m c_m(t)|\psi_{m,R(t)}\rangle$, where $\hat{H}_{R(t)}|\psi_{m,R(t)}\rangle = E_m|\psi_{m,R(t)}\rangle$. Transforming to the interaction picture, we derive

$$\frac{d}{dt}c^i_m(t) + \sum_{n\neq m} c^i_n(t)\Omega_{mn}e^{\frac{i}{\hbar}(E_m-E_n)t}\cos\omega t = 0, \tag{S38}$$

where the Rabi frequency equals:

$$\Omega_{mn} = \frac{qm_n\vec{E}_0}{M\hbar}\frac{E_m - E_n}{\hbar\omega}\cdot\langle\psi_{m,R(t)}|\vec{r}|\psi_{n,R(t)}\rangle. \tag{S39}$$

As the matrix element does not depend on t, so we write it as $\langle\psi_m|\vec{r}|\psi_n\rangle$ in Eq. (8) in the main text. In the derivation, we used the fact that $\psi_{n,R(t)}$ is a function of $\vec{r}-\vec{R}(t)$. so $\nabla_R\psi_{n,R(t)} = -\nabla_r\psi_{n,R(t)}$. Then,

$$\begin{aligned}\langle\psi_{m,R}|\nabla_R|\psi_{n,R}\rangle &= -\langle\psi_{m,R}|\nabla_r|\psi_{n,R}\rangle \\ &= -\frac{m_n}{\hbar^2}\langle\psi_{m,R}|[\vec{r},\hat{H}]|\psi_{n,R}\rangle \\ &= (E_m - E_n)\frac{m_n}{\hbar^2}\langle\psi_{m,R}|\vec{r}|\psi_{n,R}\rangle.\end{aligned} \tag{S40}$$

This completes the derivation from Eq. (S37) to the Rabi frequency expression Eq. (S39).

Numerically, we calculate the matrix element by discretizing the integral on the same lattice as described in section 1. The integral is done on a cubic region whose center is the sphere center of the nanocrystal and the length of a side is 3 times of the sphere radius. The numerical test shows that the box size of the integral gives good numerical convergence of the matrix element to three effective digits accuracy.

[1] C. R. Gould and E. I. Sharapov, Fermi's favorite figure: the history of the pseudopotential concept in atomic physics and neutron physics, The European Physical Journal H **47**, 1 (2022).

[2] V. F. Sears, Neutron scattering lengths and cross sections, Neutron news **3**, 26 (1992).

[3] G. Kresse and J. Furthmüller, Efficient iterative schemes for ab initio total-energy calculations using a plane-wave basis set, Physical review B **54**, 11169 (1996).

[4] G. Kresse and D. Joubert, From ultrasoft pseudopotentials to the projector augmented-wave method, Physical review b **59**, 1758 (1999).

[5] J. P. Perdew, K. Burke, and M. Ernzerhof, Generalized gradient approximation made simple, Physical review letters **77**, 3865 (1996).

[6] H. J. Monkhorst and J. D. Pack, Special points for brillouin-zone integrations, Physical review B **13**, 5188 (1976).

[7] A. Togo and I. Tanaka, First principles phonon calculations in materials science, Scripta Materialia **108**, 1 (2015).